


## Doping-Induced Quantum Spin Hall Insulator to Superconductor Transition

Zhenjiu Wang,<sup>1,\*</sup> Yuhai Liu<sup>2,3</sup>, Toshihiro Sato,<sup>1</sup> Martin Hohenadler<sup>1</sup>, Chong Wang,<sup>4</sup>  
Wenan Guo<sup>3,2</sup> and Fakher F. Assaad<sup>1,5,†</sup><sup>1</sup>*Institut für Theoretische Physik und Astrophysik, Universität Würzburg, 97074 Würzburg, Germany*<sup>2</sup>*Beijing Computational Science Research Center, 10 East Xibeiwang Road, Beijing 100193, China*<sup>3</sup>*Department of Physics, Beijing Normal University, Beijing 100875, China*<sup>4</sup>*Perimeter Institute for Theoretical Physics, Waterloo, Ontario N2L 2Y5, Canada*<sup>5</sup>*Würzburg-Dresden Cluster of Excellence ct.qmat, Am Hubland, 97074 Würzburg, Germany* (Received 9 July 2020; revised 19 February 2021; accepted 21 April 2021; published 20 May 2021)

A quantum spin Hall insulating state that arises from spontaneous symmetry breaking has remarkable properties: skyrmion textures of the SO(3) order parameter carry charge  $2e$ . Doping this state of matter opens a new route to superconductivity via the condensation of skyrmions. We define a model amenable to large-scale negative sign free quantum Monte Carlo simulations that allows us to study this transition. Our results support a direct and continuous doping-induced transition between the quantum spin Hall insulator and an  $s$ -wave superconductor. We can resolve dopings away from half-filling down to  $\delta = 0.0017$ . Such routes to superconductivity have been put forward in the realm of twisted bilayer graphene.

DOI: 10.1103/PhysRevLett.126.205701

**Introduction.**—Doping a band insulator generically leads to a Fermi liquid state whose Fermi surface may become unstable to superconductivity. In contrast, insulating states where correlation effects are dominant provide different routes to superconductivity. Low-lying Goldstone modes present in the insulating state can provide a glue between doped charge carriers. Spin fluctuation theories of high-temperature superconductivity follow this idea [1,2]. The correlated insulator can also contain preformed pairs that become charged upon doping. The resonating valence bond state based theory of high-temperature superconductivity follows this idea [3,4]. More recently, the idea of preformed pairs has been put forward in the realm of graphene Moiré superlattice systems [5] such as twisted bilayer graphene [6]. Here, a correlation-induced topological insulator contains skyrmions that carry charge  $2e$  as low-lying excitations [7]. Upon doping superconductivity emerges due to the condensation of charged skyrmions.

The model we consider in this Letter differs significantly from those discussed in the context of graphene Moiré superlattice systems but captures the essence of the aforementioned topological route to superconductivity. In Ref. [8], we introduced a model of Dirac fermions supplemented with a next-nearest-neighbor interaction term ( $\sim\lambda$ ) and investigated its phase diagram at half-filling (see Fig. 1). The interaction dynamically generates a quantum spin Hall (QSH) insulating state that breaks SU(2) spin rotational symmetry.

Upon further increasing  $\lambda$  at half-filling, the QSH state gives way to an  $s$ -wave superconductor (SSC). The QSH SSC transition falls into the class of deconfined quantum critical points (DQCPs) [7]. Our previous work [8] suggests

that both phase transitions are described by conformal field theories. The semimetal to QSH transition is in the Gross-Neveu-Yukawa universality class [11] whereas the DQCP is associated with a noncompact CP<sup>1</sup> [12] field theory describing the fractionalized SO(3) order parameter.

The insulating QSH state has both preformed pairs, corresponding to skyrmions of the QSH order parameter, and Goldstone modes. Understanding the fate of this state as a function of doping is the aim of this Letter. Our results are consistent with a doping-induced weakly first-order or continuous QSH SSC transition driven by the condensation of skyrmions.

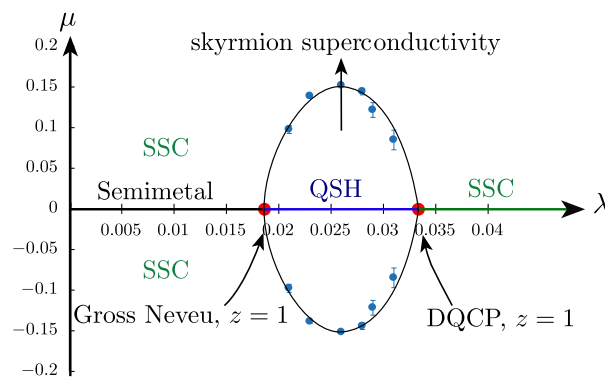


FIG. 1. Phase diagram of the model of Eq. (1) in the interaction strength  $\lambda$  versus chemical potential plane. The data at half-filling are reproduced from Ref. [8]. The critical chemical potential  $\mu_c$  for the transition from the quantum spin Hall (QSH) to the  $s$ -wave superconductor (SSC) is computed by measuring the pairing gap at half-filling [see Ref. [9] and Fig. 3(a)].

*Model and method.*—We consider a model of Dirac fermions in  $2 + 1$  dimensions on the honeycomb lattice with Hamiltonian

$$\hat{H} = -t \sum_{\langle i,j \rangle} (\hat{c}_i^\dagger \hat{c}_j + \text{H.c.}) - \lambda \sum_{\square} \left( \sum_{\langle\langle ij \rangle\rangle \in \square} \hat{J}_{ij} \right)^2 \quad (1)$$

with  $\hat{J}_{ij} = i\nu_{ij} \hat{c}_i^\dagger \boldsymbol{\sigma} \hat{c}_j + \text{H.c.}$  The spinor  $\hat{c}_i^\dagger = (\hat{c}_{i,\uparrow}^\dagger, \hat{c}_{i,\downarrow}^\dagger)$  where  $\hat{c}_{i,\sigma}^\dagger$  creates an electron at lattice site  $i$  with  $z$  component of spin  $\sigma$ . The first term accounts for nearest-neighbor hopping. The second term is a plaquette interaction involving next-nearest-neighbor pairs of sites and phase factors  $\nu_{ij} = \pm 1$  identical to the Kane-Mele model [13], see also Ref. [8]. Finally,  $\boldsymbol{\sigma} = (\sigma^x, \sigma^y, \sigma^z)$  correspond to the Pauli spin matrices. We used the ALF (algorithms for lattice fermions) implementation [14] of the auxiliary-field quantum Monte Carlo (QMC) method [15–17]. Because  $\lambda > 0$ , we can use a real Hubbard-Stratonovich decomposition for the perfect square term. For each field configuration, time-reversal symmetry is present, even at finite chemical potential, so that eigenvalues of the fermion matrix occur in complex conjugate pairs. Hence, we do not suffer from the negative sign problem. In contrast to Ref. [8], we used a projective version of the algorithm (PQMC) [17–19]. The PQMC is a canonical approach in which the ground state is filtered out of a trial wave function that is chosen to be a Slater determinant. To avoid the negative sign problem, the trial wave function has to be time-reversal symmetric, so that we can only dope away from half-filling with Kramers pairs. For the considered trial wave function (see Ref. [9] for further details), we observed that a projection parameter set by the linear length of the lattice is sufficient to reach the ground state.

*Mean-field approaches.*—Before discussing our QMC results, it is instructive to carry out a mean-field approximation. When expanding the square in Eq. (1), diagonal terms  $\hat{J}_{ij}^2$  contain, among other interactions,  $s$ -wave pair hopping terms that permit us to introduce an SSC order parameter. The off-diagonal terms allow for QSH ordering (see Ref. [9] for a detailed calculation). As seen in Fig. 2, doping the semimetal produces the SSC. This reflects the pairing instability of Fermi surfaces to attractive interactions within Bardeen-Cooper-Schrieffer theory. The protecting symmetries of the QSH state are related to time reversal and global charge conservation. Hence, the coexistence region (QSH + SSC) is topologically trivial. Furthermore, the transition at half-filling from the QSH to QSH + SSC is continuous and does not require the closing of the single-particle gap. Upon doping, the mean-field approximation generically supports two scenarios: (i) a continuous transition with dynamical exponent  $z = 2$  from the QSH to QSH + SSC, (ii) a first-order transition from the QSH to SSC [20]. Our mean-field approximation provides examples of both scenarios. As expected, it fails to

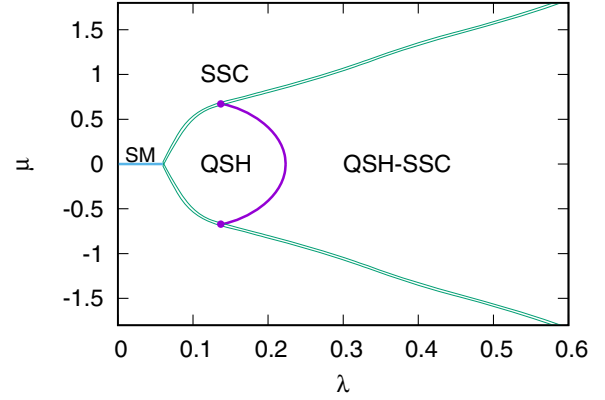


FIG. 2. Mean-field ground-state phase diagram. The blue and purple (green) lines correspond to continuous (first-order) transitions.

capture the DQCP between the QSH and SSC phases at half-filling [8].

*QMC results.*—We now turn to unbiased QMC results which, in contrast to the mean-field approach, capture Goldstone modes as well as topological skyrmion excitations. We consider  $t = 1$  and  $\lambda = 0.026$ , which places us in the center of the QSH phase at half-filling.

At this filling, we show in Fig. 3 the momentum dependence of the spin-orbit coupling gap  $\Delta_{\text{QSH}}(\mathbf{q})$  and the SSC gap  $\Delta_{\eta}(\mathbf{q})$ . To obtain these data, we measured the imaginary-time displaced correlation functions of the spin-orbit coupling operators  $\hat{\mathcal{O}}_{\mathbf{r},n}^{\text{QSH}} = \hat{J}_{\mathbf{r}+\delta_n, \mathbf{r}+\eta_n}$ . Here,  $\mathbf{r}$  denotes a unit cell and  $n$  runs over the six next-nearest neighbor bonds of the corresponding hexagon with legs  $\mathbf{r} + \delta_n$  and  $\mathbf{r} + \eta_n$ . We also consider the  $s$ -wave pairing operators  $\hat{\eta}_{\mathbf{r},\tilde{\delta}}^+ = \hat{c}_{\mathbf{r}+\tilde{\delta},\uparrow}^\dagger \hat{c}_{\mathbf{r}+\tilde{\delta},\downarrow}^\dagger$ , where  $\tilde{\delta}$  runs over the two orbitals in unit cell  $\mathbf{r}$ . The gaps were obtained from

$$\begin{aligned} S^{\text{QSH}}(\mathbf{q}, \tau) &= \sum_n \langle \hat{\mathcal{O}}_{\mathbf{q},n}^{\text{QSH}}(\tau) \hat{\mathcal{O}}_{-\mathbf{q},n}^{\text{QSH}}(0) \rangle \propto e^{-\Delta_{\text{QSH}}(\mathbf{q})\tau}, \\ S^{\text{SSC}}(\mathbf{q}, \tau) &= \sum_{\tilde{\delta}} \langle \hat{\eta}_{\mathbf{q},\tilde{\delta}}^+(\tau) \hat{\eta}_{\mathbf{q},\tilde{\delta}}^-(0) + \hat{\eta}_{\mathbf{q},\tilde{\delta}}^-(\tau) \hat{\eta}_{\mathbf{q},\tilde{\delta}}^+(0) \rangle, \\ &\propto e^{-\Delta_{\eta}(\mathbf{q})\tau}, \end{aligned} \quad (2)$$

in the limit of large imaginary time  $\tau$  [9]. As expected for a Goldstone mode,  $\Delta_{\text{QSH}}(\mathbf{q})$  in Fig. 3(b) exhibits a gapless, linear dispersion around the ordering wave vector  $\mathbf{q} = \Gamma$ . On the other hand,  $\Delta_{\eta}(\mathbf{q})$  remains clearly nonzero with quadratic dispersion [see Fig. 3(a)]. It is also important to note that an  $s$ -wave pair has a smaller excitation energy than twice the single-particle gap, as shown in the inset of Fig. 3(a). Thus, pairing is present and we can foresee that these preformed pairs will condense to form a superconducting state upon doping.

A key quantity to understand the nature of the metal or superconductor to insulator transition is the behavior of

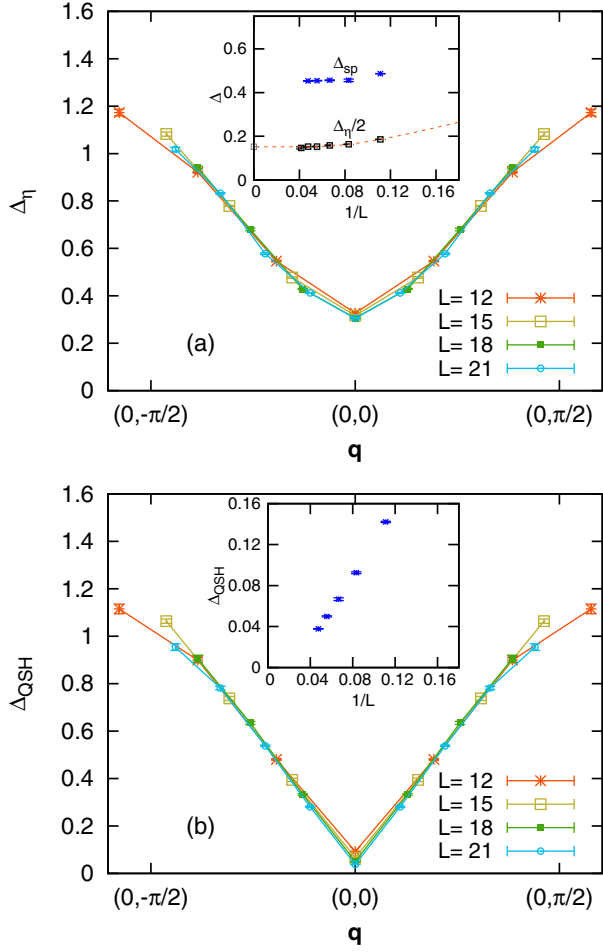


FIG. 3. Momentum dependence of (a) the pairing gap and (b) the QSH gap for the half-filled case, in the vicinity of the  $\Gamma$  point along the direction toward the  $M$  point in the Brillouin zone of the honeycomb lattice. The inset of (a) shows the  $1/L$  dependence of the single-particle gap  $\Delta_{\text{SP}}$  and half of the  $s$ -wave pairing gap  $\Delta_{\eta}/2$ . The inset of (b) shows the QSH gap,  $\Delta_{\text{QSH}}$ , versus  $1/L$ .

the chemical potential upon doping away from half-filling [21–23]. For first-order transitions,  $\mu$  shows a jump. For continuous transitions, and with the assumption of a single length scale, the singular part of the free energy scales as  $f \propto |\mu - \mu_c|^{\nu(d+z)}$  with  $d$  the dimensionality and  $\nu$  ( $z$ ) the correlation length (dynamical) exponent. Since the doping defined as  $1 - n$  is proportional to  $\partial f / \partial \mu$  and the compressibility is associated with twisting boundaries in the imaginary-time direction, one can show that for transitions driven via the chemical potential the hyperscaling relation  $\nu z = 1$  holds. Thereby,  $\delta \propto |\mu - \mu_c|^{\nu d}$ . Doping a band insulator satisfies the hyperscaling assumption. For a quadratic band,  $z = 2$  so that  $\delta \propto |\mu - \mu_c|^{d/2}$ . This scaling behavior is satisfied upon doping a bosonic Mott insulator [23].

With the PQMC, we can compute the ground-state energy for a given, even particle number  $N_p$  and then derive the chemical potential. However, we found it more

efficient to extract  $\mu$  from an estimate of  $\Delta_{\eta^-}(N_p)$  by analyzing the long imaginary-time behavior of the pair correlation function  $\sum_{\delta} \langle \hat{\eta}_{q,\delta}^+(\tau) \hat{\eta}_{q,\delta}^-(0) \rangle \sim e^{-\Delta_{\eta^-} \tau}$ , where  $q = \Gamma$ . In particular,

$$\mu \equiv \frac{E(N_p) - E(N_p - 2)}{2} = \frac{\Delta_{\eta^-}(N_p)}{2}. \quad (3)$$

With the doping relative to half-filling defined as  $\delta \equiv 1 - [(N_p - 1)/2L^2]$  [24], we obtain the data shown in Fig. 4. For alternative ways of computing  $\mu$  see the Supplemental Material [9].

Figure 4 plots  $\delta$  as a function of  $\mu$ . The vertical dash-dotted line corresponds to the critical chemical potential. The data support a linear behavior for  $\mu > 0.16$ , but this form would overshoot the critical chemical potential. In a narrow window of dopings,  $\delta < 0.01$ , we observe a downturn in the functional form. Within our precision, we can offer two interpretations: a weakly first-order transition or a continuous transition with dynamical exponent  $z > 2$ . We note that continuous metal-insulator transitions with  $z > 2$  have been put forward in the context of doped quantum antiferromagnets [21,25].

Another important question to answer is if the onset of superconductivity is tied to the vanishing of the QSH order parameter. To this end, we consider the renormalization-group invariant correlation ratios ( $\alpha = \text{QSH, SSC}$ )

$$R_{\alpha} \equiv 1 - \frac{S^{\alpha}(\mathbf{q}_0 + \delta \mathbf{q})}{S^{\alpha}(\mathbf{q}_0)} \quad (4)$$

based on the equal-time correlation functions of the spin current and  $s$ -wave paring operators in momentum space,  $S^{\alpha}(\mathbf{q})$ . Here,  $\mathbf{q}_0 = (0, 0)$  is the ordering wave

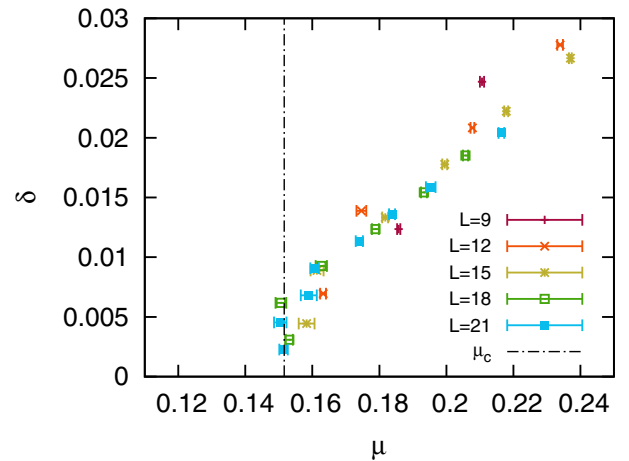


FIG. 4. Doping factor  $\delta$  as a function of chemical potential  $\mu \equiv \Delta_{\eta^-}/2$  for sizes  $L = 9, 12, 15, 18,$  and  $21$ . The red dashed line is the critical chemical potential from the extrapolated pairing gap  $\Delta_{\eta^-}/2$  shown in Fig. 3.

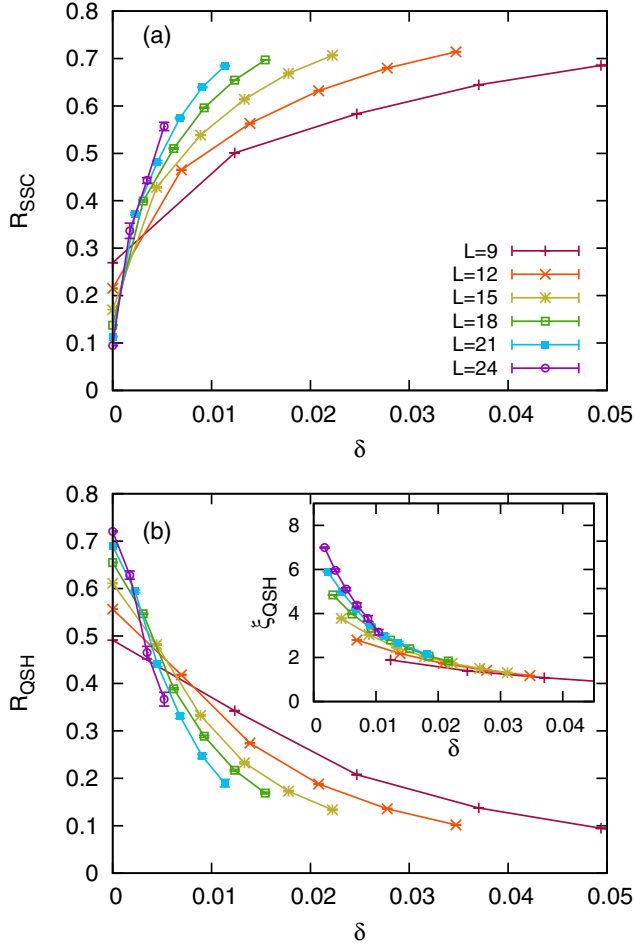


FIG. 5. Correlation ratios for (a) SSC and (b) QSH orders as a function of doping  $\delta$ . The system sizes are  $L = 9, 12, 15, 18, 21$ , and  $24$ . The inset of (b) shows the  $\delta$  dependence of the finite-size correlation length for the QSH order parameter.

vector and  $\mathbf{q}_0 + \delta\mathbf{q}$  a neighboring wave vector. By definition,  $R_\alpha \rightarrow 1$  ( $\rightarrow 0$ ) in the ordered (disordered) state for  $L \rightarrow \infty$ . At a critical point,  $R_\alpha$  is scale invariant and for sufficiently large  $L$ , one should observe a crossing in  $R_\alpha$  for different system sizes. Figures 5(a) and 5(b) show results for  $R_{\text{SSC}}$  and  $R_{\text{QSH}}$  as a function of  $\delta$ . Because of the observed binding of electrons in the insulating state, we expect superconductivity for any  $\delta > 0$ . This is confirmed by Fig. 5(a). The drift in the crossings due to corrections to scaling is consistent with  $\delta_c^{\text{SSC}} \rightarrow 0$  in the thermodynamic limit. The same quantity is plotted for the QSH correlation ratio in Fig. 5(b). The data show that the QSH order parameter vanishes very rapidly as a function of doping. Again, the drift of the crossing point as a function of system size scales to smaller values of  $\delta$ . Given the data, we can provide an upper bound  $\delta_c^{\text{QSH}} < 0.0017$  which corresponds to our resolution [26]. In our interpretation of Fig. 4, we could not exclude the possibility of a weakly first-order transition. On our finite systems, neither of the

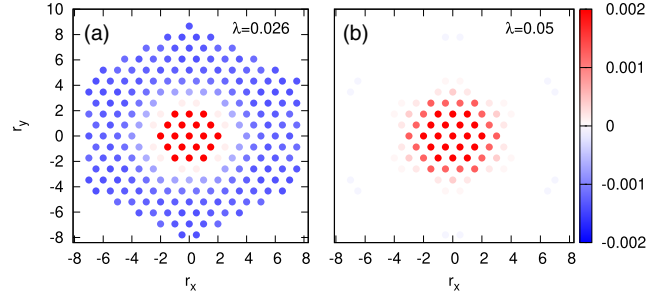


FIG. 6. Real-space equal-time correlation function of the QSH order parameter around a pinned hole pair at the origin. Hamiltonian (1) was supplemented with a pinning potential  $\hat{H}_{\text{pin}} \equiv C \sum_r \sum_{\delta} e^{-|r+\delta|/\xi} \hat{c}_{r+\delta}^\dagger \hat{c}_r$  with  $C = 1$  and  $\xi = 1$ . We consider  $L = 15$ , at (a)  $\lambda = 0.026$  and (b)  $\lambda = 0.05$ .

correlation ratios show a discontinuity, consistent with a continuous transition.

As a cross-check, we consider the second-moment, finite-size correlation length [27],  $\xi_\alpha^2 \equiv \{[\sum_r |r|^2 S^\alpha(r)] / [\sum_r S^\alpha(r)]\}$ , obtained from the real-space, equal-time correlation functions [28]. The inset of Fig. 5(b) reveals the absence of saturation of the QSH correlation length for  $\delta > 0.0017$ . Saturation would be expected for a first-order transition.

The notion of skyrmion superconductivity hinges on a locking in of the charge density and texture of the SO(3) QSH order parameter. To image this, we dope two holes away from half-filling and localize them by modulating the chemical potential. The real space correlations of the QSH order parameter are then expected to show a texture akin to a skyrmion. Precisely this is seen in Fig. 6(a) at  $\lambda = 0.026$ . In contrast, *far* away from the QSH state at  $\lambda = 0.05$  [see Fig. 6(b)] a skyrmion, is not present around the localized pair.

*Discussion and summary.*—Our data suggest a doping-induced, continuous, and direct phase transition between the QSH state and the SSC. Clearly, we cannot exclude the possibility of a weakly first-order transition in which the correlation length saturates beyond our maximum system size ( $L = 24$ ). Our dynamically generated QSH state possesses Goldstone modes and charge- $2e$  skyrmions of the QSH order parameter. The Goldstone modes correspond to long-wavelength fluctuations of the spin-orbit coupling and do not break time-reversal symmetry. Hence, single-particle spin-flip scattering off Goldstone modes—as present in doped quantum antiferromagnets—is not allowed. Remarkably, one can also show that  $[\hat{c}_{\mathbf{k}=0}, \hat{H}_\lambda] = 0$  (see Ref. [9]), so that at the  $\Gamma$  point the single-particle spectral function [9] is unaffected by the interaction  $\hat{H}_\lambda$ . This is in strong contrast to quantum antiferromagnets, where Goldstone modes couple to single-particle excitations to form a narrow band of spin polarons [29–31]. These arguments suggest that Goldstone modes do not provide the glue that leads to pairing.

We interpret our results in terms of preformed pairs, skyrmions carrying charge  $2e$ , that condense upon doping. In fact, by pinning the charge we were able to image the skyrmion. Within this picture, the correlation length that diverges at the transition corresponds to the average distance between skyrmions.

The finite-temperature phase diagram remains to be analyzed. Such calculations could reveal pseudogap physics related to preformed pairs at small doping. At large dopings, a crossover to conventional superconductivity is expected.

F. F. A. acknowledges many insightful discussions with M. Imada on the topic of metal-insulator transitions. Z. W. would like to thank M. Ulybyshev and X. Wu for useful discussions on twisted bilayer graphene. The authors gratefully acknowledge the Gauss Centre for Supercomputing e.V. for funding this project by providing computing time on the GCS Supercomputer SUPERMUC-NG at Leibniz Supercomputing Centre. F. F. A. thanks the Deutsche Forschungsgemeinschaft for funding under Grant No. AS 120/15-1 as well as the Würzburg-Dresden Cluster of Excellence on Complexity and Topology in Quantum Matter ct.qmat (EXC 2147, Project No. 390858490). Z. W. is thankful for financial support from the DFG funded SFB 1170 on Topological and Correlated Electronics at Surfaces and Interfaces. T. S. thanks the Deutsche Forschungsgemeinschaft for funding under Grant No. SA 3986/1-1. Y. L. was supported by the China Postdoctoral Science Foundation under Grants No. 2019M660432 as well as the National Natural Science Foundation of China under Grants No. 11947232 and No. U1930402. Research at Perimeter Institute (C.W.) is supported by the Government of Canada through the Department of Innovation, Science and Economic Development Canada and by the Province of Ontario through the Ministry of Research, Innovation and Science. W. G. was supported by the National Natural Science Foundation of China under Grants No. 11775021 and No. 11734002.

\*Zhenjiu.Wang@physik.uni-wuerzburg.de

†assaad@physik.uni-wuerzburg.de

- [1] R. Coldea, S. M. Hayden, G. Aeppli, T. G. Perring, C. D. Frost, T. E. Mason, S.-W. Cheong, and Z. Fisk, *Phys. Rev. Lett.* **86**, 5377 (2001).
- [2] D. J. Scalapino, *Rev. Mod. Phys.* **84**, 1383 (2012).
- [3] P. W. Anderson, *Science* **235**, 1196 (1987).
- [4] P. A. Lee, N. Nagaosa, and X. G. Wen, *Rev. Mod. Phys.* **78**, 17 (2006).
- [5] Y.-H. Zhang, D. Mao, Y. Cao, P. Jarillo-Herrero, and T. Senthil, *Phys. Rev. B* **99**, 075127 (2019).
- [6] E. Khalaf, S. Chatterjee, N. Bultinck, M. P. Zaletel, and A. Vishwanath, [arXiv:2004.00638](https://arxiv.org/abs/2004.00638).
- [7] T. Grover and T. Senthil, *Phys. Rev. Lett.* **100**, 156804 (2008).
- [8] Y. Liu, Z. Wang, T. Sato, M. Hohenadler, C. Wang, W. Guo, and F. F. Assaad, *Nat. Commun.* **10**, 2658 (2019).
- [9] See Supplemental Material at <http://link.aps.org/supplemental/10.1103/PhysRevLett.126.205701> for more details, which includes Ref. [10].
- [10] F. F. Assaad and M. Imada, *J. Phys. Soc. Jpn.* **65**, 189 (1996).
- [11] D. J. Gross and A. Neveu, *Phys. Rev. D* **10**, 3235 (1974).
- [12] T. Senthil, A. Vishwanath, L. Balents, S. Sachdev, and M. P. Fisher, *Science* **303**, 1490 (2004).
- [13] C. L. Kane and E. J. Mele, *Phys. Rev. Lett.* **95**, 146802 (2005).
- [14] M. Bercx, F. Goth, J. S. Hofmann, and F. F. Assaad, *SciPost Phys.* **3**, 013 (2017).
- [15] R. Blankenbecler, D. J. Scalapino, and R. L. Sugar, *Phys. Rev. D* **24**, 2278 (1981).
- [16] S. R. White, D. J. Scalapino, R. L. Sugar, E. Y. Loh, J. E. Gubernatis, and R. T. Scalettar, *Phys. Rev. B* **40**, 506 (1989).
- [17] F. Assaad and H. Evertz, in *Computational Many-Particle Physics, Lecture Notes in Physics* Vol. 739, edited by H. Fehske, R. Schneider, and A. Weiße (Springer, Berlin Heidelberg, 2008), pp. 277–356.
- [18] G. Sugiyama and S. Koonin, *Ann. Phys. (N.Y.)* **168**, 1 (1986).
- [19] S. Sorella, S. Baroni, R. Car, and M. Parrinello, *Europhys. Lett.* **8**, 663 (1989).
- [20] An intermediate metallic state would be unstable to pairing and we have excluded fine-tuning.
- [21] M. Imada, A. Fujimori, and Y. Tokura, *Rev. Mod. Phys.* **70**, 1039 (1998).
- [22] F. F. Assaad and M. Imada, *Phys. Rev. B* **58**, 1845 (1998).
- [23] M. P. A. Fisher, P. B. Weichman, G. Grinstein, and D. S. Fisher, *Phys. Rev. B* **40**, 546 (1989).
- [24] Here,  $N_p - 1$  is the thermal average of particle numbers, with the  $N_p$  and the  $N_p - 2$  sector tuned to have the same ground-state energy at the chemical potential defined in Eq. (3).
- [25] F. F. Assaad and M. Imada, *Phys. Rev. Lett.* **76**, 3176 (1996).
- [26] Since we are working in the canonical ensemble, the smallest doping is set by  $2/(2L^2)$ .
- [27] F. Parisen Toldin, M. Hohenadler, F. F. Assaad, and I. F. Herbut, *Phys. Rev. B* **91**, 165108 (2015).
- [28] The fact that there is no additional phase factor in the above summations comes from the known ordering wave vector  $\mathbf{k} = \Gamma$ .
- [29] G. Martinez and P. Horsch, *Phys. Rev. B* **44**, 317 (1991).
- [30] R. Preuss, W. Hanke, and W. von der Linden, *Phys. Rev. Lett.* **75**, 1344 (1995).
- [31] M. Raczkowski, R. Peters, T. T. Phung, N. Takemori, F. F. Assaad, A. Honecker, and J. Vahedi, *Phys. Rev. B* **101**, 125103 (2020).